ACS APPLIED POLYMER MATERIALS

pubs.acs.org/acsapm Article

Poly(butylene succinate)-Based Composites with Technical and Extracted Lignins from Wood Residues

Elodie Melro,* Hugo Duarte, Alireza Eivazi, Carolina Costa, Maria L. Faleiro, Ana M. Rosa da Costa, Filipe E. Antunes, Artur J. M. Valente, Anabela Romano, Magnus Norgren, and Bruno Medronho

Cite This: *ACS Appl. Polym. Mater.* 2024, 6, 1169−1181 Read Online

ACCESS | Metrics & More | Article Recommendations | Supporting Information

ABSTRACT: Poly(butylene succinate) (PBS) has been drawing attention as a reliable biodegradable and sustainable alternative to synthetic petroleum-based polymers. In this study, PBS-lignin composites were developed using a recently extracted lignin (LA-lignin) from pine wood residues employing an innovative sustainable approach. These composites were systematically compared with PBS-based composites formed with commonly used technical lignins. The molecular weight of the lignins was evaluated, along with various structural and performance-related properties. The LA-lignin/PBS composites display a remarkably low water solubility (ca. < 2%), water uptake (<ca. 1%), and high contact angle (>ca. 100°). Moreover, the rigidity and thermal stability of the LA-lignin-PBS composites were higher than those of the systems formed with technical lignins. Although all composites studied present remarkable antioxidant features, the novel LA-lignin-PBS systems stand out in terms of antiadhesion activity against both Gram-positive and Gram-negative bacteria. Overall, the systematic analysis performed in this work regarding the impact of various lignins on the formed PBS composites enables a better understanding of the essential structural and compositional lignin features for achieving biobased materials with superior properties.

KEYWORDS: *biocomposites, bio-PBS, Poly(butylene succinate)-lignin composites, wood residues, levulinic acid-based solvent*

1. INTRODUCTION

Approximately 360 million tons of virgin plastic were produced in 2018. The generated plastic waste was ca. 250 Mt, where ca. 173 Mt is estimated to be collected for recycling and landfill purposes, while the remaining waste is improperly discarded and leached into the different ecosystems.[1] Most petroleum-derived polymers are resistant to biodegradation, which is one of the main factors contributing to the deterioration of the environment when inadequately disposed. The use of biodegradable polymers can represent a suitable sustainable alternative to reduce the negative environmental impact caused by nonbiodegradable polymers.[2]

The increasing awareness of plastic pollution and the need for biodegradable sustainable solutions have opened the path for an industrial-scale production of compostable polymers as, for example, the poly(1,4-butylene succinate) (PBS).[3] Accounting for approximately 11% of the global production of biodegradable plastics in 2017, this polymer is one of the most promising aliphatic polyesters.[4,5] PBS is a white crystalline thermoplastic with a melting point similar to low-density polyethylene (LDPE), i.e., 90 to 120 °C, glass transition temperature between polyethylene (PE) and polypropylene (PP), −45 to −10 °C, mechanical properties comparable with PP and LDPE, and stiffness features in between low- and high-density PP.[6−8] PBS can be used in different applications, such as for food packaging, agricultural mulch films, biomedical applications (e.g., controlled drug

Received: September 6, 2023
Revised: December 15, 2023
Accepted: December 29, 2023
Published: January 16, 2024

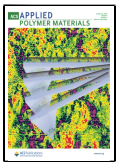

release and tissue engineering), and automotive interiors.[9−13] However, PBS presents some shortcomings, such as high price, poor tensile properties, low melt viscosity, high flammability, and low gas barrier properties, which limits its generalized use.[14−16] Nonetheless, PBS can be reinforced with several biopolymers, such as starch and natural fibers containing cellulose and lignin, reducing energy consumption for its production and improving biodegradability.[16,17]

Lignin is one of the most abundant biopolymers on earth. This amorphous and aromatic copolymer is synthesized from random polymerization of three phenylpropane monomers: coumaryl, coniferyl, and sinapyl alcohols.[18] Its structure, molecular weight, chemical reactivity, and chemical composition are strongly dependent on the source and extraction process.[19,20] Lignin is generally regarded as a byproduct mainly from pulp and paper industries,[21] but it presents many appealing features, such as high biocompatibility, degradability, and antibacterial, antifungal and antioxidant properties.[22] Due to the growing awareness to produce and consume sustainable materials, the exploration of new value-added products using lignin has becoming very appealing, and novel strategies to valorize this aromatic polymer have emerged.[23,24] Lignin-based composites can be used in several areas, such as sensors, energy storage systems, responsive material, functional packaging, and biomedical materials.[25] Lignin has been recently used to improve some properties of neat PBS, as reducing flammability and smoke release, enhancing mechanical performance, conferring UV-shielding features, and introducing antioxidant and antimicrobial properties.[26−30] Some technical lignins have been used to produce PBS-lignin composites, such as alkali lignin, kraft lignin, and lignosulfonate.[15,30,31] However, to the best of our knowledge, it is notable that a systematic comparative study has been lacking in the literature. Therefore, in this work, we systematically assessed the performance of PBS-based composites with various technical lignins and compared them with the effects induced by the lignin extracted from pine wood residues using a sustainable levulinic acid-based process recently introduced by us.[32−34] The molecular weight of all lignins used was estimated by size exclusion chromatography, and a thorough structural and performance characterization was performed on the PBS-lignin composites, involving torque rheometry, infrared spectroscopy, thermogravimetric analysis, contact angle and water solubility, scanning electron microscopy, X-ray diffraction, and atomic force microscopy. The mechanical and antioxidant properties were also evaluated for all composites. This work is expected to not only highlight a lignin type extracted from wood residues using a sustainable process but also feature it in the development of novel lignin-PBS composites while comparing it with commercially available lignins.

2. MATERIALS AND METHODS

2.1. Materials. BioPBS FZ71PM (from now on simply referred to as PBS) is food contact grade, approved by FDA and was acquired from MCCP. The PBS has a density of 1.26 g cm^{-3} (ISO 1183), melting temperature of 115 °C (ISO 3146), melt flow index of 22 (ISO 1133) and yield stress, stress at break, and strain at break (ISO 527-2) of 40 MPa, 30 MPa, and 170%, respectively. Dealkaline lignin (M_w = 10,263 Da), alkali lignin (M_w = 6024 Da), sodium lignosulfonate (M_w = 4881 Da), and 2,2-diphenyl-1-picrylhydrazyl (≥97.0%) (DPPH) free radical were purchased from Tokyo Chemical Industry (TCI). Methanol was obtained from José Manuel Gomes dos Santos, Lda. (Porto, Portugal), levulinic acid (98%) from Sigma-Aldrich, and hydrochloric acid (37%) from Fisher Scientific. Maritime pine (*Pinus pinaster* Ait.) sawdust was received as a kind gift from Valco—Madeiras e Derivados, S.A. (Leiria, Portugal). Pullulan standards were purchased from PSS Polymer Standards (Agilent); dimethylformamide (DMF) [high-performance liquid chromatography (HPLC) grade] was obtained from Sigma-Aldrich, and lithium chloride was acquired from Fluka. Hydrophilic 0.45 μm filter disks were obtained from Labfil. Phosphate buffer saline was prepared in situ with sodium chloride from Fluka (Buchs, Switzerland), potassium chloride and potassium phosphate monobasic from Merk (Darmstadt, Germany), and sodium phosphate dibasic from Sigma-Aldrich (Steinheim, Germany). Glutaraldehyde 25% aqueous solution was obtained from Merk (Darmstadt, Germany). Cultures of *Staphylococcus aureus* (*S. aureus*) (DSM 346) and *Escherichia coli* (*E. coli*) (DSM 1077) were grown on tryptic soy broth (TSB) from Biokar Diagnostics (Paris, France).

2.2. Extraction of Lignin from Pine Wood Sawdust. Apart from the technical lignins used, one has also extracted lignin from pine wood residues following the procedure introduced and described by us.[34] In brief, LA-lignin is obtained after performing pine wood fractionation using levulinic acid as the solvent. The extraction is performed over 2 h at 140 °C using 0.1 M HCl as the inorganic catalyst. The obtained lignin, henceforth simply termed LA-lignin, has a M_w of 2970 Da. Detailed information on LA-lignin preparation, structure, and properties can be found in the reports by Melro et al.[34] Data suggest that condensed OH structures and acidic groups are present in LA-Lignin. Moreover, the LA-lignin is enriched in C═O groups possibly originated from the partial OH-esterification with LA. The presence of guaiacyl units (G-units), C5-substituted condensed G-units, and almost no aliphatic OH groups are also worth mentioning structural features of LA-lignin. The phenolic hydroxyl content is estimated to be 0.56 mmol g^{-1}.

2.3. Size Exclusion Chromatography Analysis. Lignin samples were analyzed by size exclusion chromatography (SEC) in a modular system comprising a Biotech Degasi GPC degasser, a Waters 515 HPLC pump, an Elder CH-150 column oven, and a Knauer K-2300 refractive index detector. Two Shodex SB-806 M HQ 300 × 8.0 mm columns were used in series with a 50 × 6.0 mm OHpak SB-G 6B guard column. DMF containing 20 mM of LiCl was used as the mobile phase at 1 mL min^{-1} and 40 °C. The samples were dissolved in the eluent at 5 mg mL^{-1} (samples with lignosulfonate and alkali required heating at 70 °C for 90 min to achieve a partial solubilization) and filtered through a 0.45 μm filter disk. A conventional calibration curve was set using pullulan standards dissolved at 2 mg mL^{-1} in the eluent.

2.4. Optical Microscopy. A Kern Optics OBN 135 microscope was used to observe the lignin particles. The dry lignin powder was placed on a glass slide before imaging. Images were analyzed at 4× magnification and processed by using S-EYE 1.9.20 software.

2.5. Preparation of PBS-Based Composites. The PBS-lignin composites were prepared in a two-roll mill blender (Thermo Scientific, Haake polylab QC). In brief, the neat PBS was first melted at 130 °C for 3 min, and then the different lignins were added until constant torque was observed (i.e., after 10−15 min). After this, the composites were hot-pressed, using hot press equipment (Tecnocanto) at 130 °C for 2 min, with an applied pressure of 20 MPa.

2.6. Water Absorption and Solubility. Water absorption capacity (W_a) was analyzed following the ASTM standard D570-98.[35] Squared composite specimens (2 × 2 × 0.1 mm) were predried in an oven at 50 °C for 24 h, cooled to room temperature in a desiccator, and weighed (W_0). The samples were immersed in 50 mL of distilled water at room temperature. The experiment involved periodically measuring the sample weight gain (W_1) as a function of immersion time for 57 h. Any extra drops of water were wiped off from the composite surface prior to weighing, and tests were performed in triplicate. The W_a was calculated as

$$W_a = \frac{W_1 - W_0}{W_0} \times 100\% \quad (1)$$

https://doi.org/10.1021/acsapm.3c02103
ACS Appl. Polym. Mater. 2024, 6, 1169−1181

All swollen samples from water absorption tests were used to calculate the water solubility (W_s) via ASTM standard D570-98. In brief, the swollen samples (i.e., after 57 h immersion) were dried in an oven at 60 °C for 24 h, cooled to room temperature in a desiccator, and weighed (W_2) until they attained the equilibrium. Trials were performed in triplicate. The water solubility was calculated as

$$W_s = \frac{W_0 - W_2}{W_0} \times 100\% \quad (2)$$

Statistical analysis was performed using one-way ANOVA (α = 0.05).

2.7. Contact Angle. The water contact angle measurements were performed using the sessile drop method in a contact angle meter, Attension Theta Flex (Biolin Scientific). Images were recorded for 5 s at 10% (33 FPS). The hot-pressed composites were fixed on the movable sample plate, and 8 μL of water was dropped onto the composite surface. Ten tests for each sample were performed and averaged. Statistical analysis was performed using one-way ANOVA (α = 0.05).

2.8. Antioxidant Properties. A DPPH-based method was employed to estimate the antioxidant activity (procedure adapted from Alzagameem et al.[36]). The composite was cut into small pieces (0.2 g) and immersed in 4 mL of methanol for 24 h at room temperature. Then, the samples were centrifuged (2 min at 3000 rpm), and 1.5 mL of supernatant was mixed with 1.5 mL of 50 mg L^{-1} of DPPH in methanol. The mixture was maintained at room temperature in the dark for 60 min, and then the absorbance (A_{sample}) was measured on a UV−vis spectrophotometer (Shimadzu UV-2450) at 517 nm. The mixture of 1.5 mL of methanol and 1.5 mL of 50 mg L^{-1} DPPH in methanol was used as control. Trials were performed in triplicate, and statistical analysis was performed using one-way ANOVA (α = 0.05). The radical scavenging activity (RSA) was calculated as

$$\mathrm{RSA} = \frac{A_{control} - A_{sample}}{A_{control}} \times 100\% \quad (3)$$

2.9. Fourier Transform Infrared Spectroscopy. Infrared spectra of the different composites were recorded with a Thermo Nicolet 380 Fourier transform infrared (FT-IR) apparatus (Thermo Scientific) equipped with a Smart Orbit Diamond ATR system. The spectra were obtained in absorbance mode from 4000 to 400 cm^{-1}, with a total of 68 scans and a resolution of 8 cm^{-1}. The background spectrum was collected with air before analyzing each sample.

2.10. Mechanical Properties. The mechanical properties of the PBS-lignin composites were evaluated using a Texture Analyzer TA.XT plus (Stable Micro Systems) following the ASTM D638 standard.[37] Tensile grips of 35 mm were used to hold the composite specimens. The initial distance between the grips was 40 mm, and the velocity was set to 1 mm min^{-1}. Three samples were analyzed for each system, and statistical analysis was performed using one-way ANOVA (α = 0.05).

2.11. Thermogravimetric Analysis. Thermograms were obtained using a thermogravimetric analyzer, TG 209 F Tarsus (NETZSCH Instruments). In brief, ca. 3 mg of each composite was weighed in alumina pans and heated from 25 to 600 °C, with a heating rate of 10 °C min^{-1} under a N_2 atmosphere (flow rate of 50 mL min^{-1}).

2.12. Scanning Electron Microscopy. Field emission scanning electron microscopy (FE-SEM) imaging of the samples was carried out using a TESCAN MAIA3 electron microscope in secondary electrons mode. The accelerating voltage was 3 kV, and the working distance was set to 8 mm. Before image acquisition, the samples were coated with 6 nm Iridium using a Quorum Q150T ES.

A VEGA3 SBH from a TESCAN scanning electron microscope was used to observe the microstructure of the composites without bacteria. The sampleswere deposited on the carbon tape on the support and sputtered with a ca. 6 nm thin Au/Pd film, by cathodic pulverization using an SPI Module Sputter Coated, for 90 s at a current of 15 mA. The accelerating voltage used ranged from 5 to 15 kV, and the work distance was set to 10 mm.

2.13. Atomic Force Microscopy. Surface morphology and roughness of the samples were analyzed by atomic force microscopy (AFM; Park Systems NX20, Korea). The AFM was operated in a noncontact mode in air. A PPP-NCHR probe (Park Systems, Korea) with a nominal resonance frequency of 330 kHz and a force constant of 42 N m^{-1} was used. AFM images of 10 × 10 μm^2 representative areas on the samples were acquired with a scan rate of 0.3−0.6 Hz. The surface roughness parameter, R_q, was determined from the data using Park systems' XEI 1.8.5 image analysis software. Sample preparation for bacteria adhesion into the composites was performed by adding approximately 20 μL of a cellular culture (109 cfu mL^{-1}) which was dropped into the composite, let to dry overnight, and fixed with 2.5 wt % glutaraldehyde.

2.14. X-ray Diffraction Analysis. X-ray diffraction (XRD) was conducted at room temperature using a Bruker D2 Phaser diffractometer with Cu Kα radiation (wavelength 1.54 Å) at 30 kV and 10 mA, in $\theta - 2\theta$ geometry. The increment was fixed at 0.02°. The samples were analyzed by placing them on a silicon single crystal specially cut to provide a low background free from any interfering diffraction peaks. The thickness and solid content of the samples were almost identical, with less than 5% variation.

2.15. Bacterial Adhesion. Gram-positive *S. aureus* (DSM 346) and Gram-negative *E. coli* (DSM 1077) were chosen as model microorganisms. Bacterial growth was performed overnight at 37 °C in TSB from choosing a well-defined and characterized bacterial colony from an agar plate streak. After this, a dilution series was performed to achieve a bacterial suspension of ca. 10^4 to 10^5 cfu mL^{-1}. This inoculum was transferred to a 6-well plate in which each PBS composite was immersed for 24 h at room temperature. Each composite was previously treated for 30 min at 100 °C to reduce the probability of contamination. The bacterial culture was removed, and composites were then gently washed with phosphate buffer, transferred to falcon tubes with 1 mL of buffer, and vortexed to remove the attached cells. A dilution series from the buffer containing the bacteria detached from the composites was made, and bacterial counts were performed.[38]

3. RESULTS AND DISCUSSION

3.1. Mixing PBS and Lignin. The addition of lignin to melted PBS promotes an initial increase in torque due to the material resistance. During homogenization of the PBS and lignin mixtures, torque decreases and a steady state is eventually obtained. The PBS-dealkaline lignin mixture was selected to illustrate the general behavior of the equilibrium torque as a function of lignin content (Figure S1). Similar profiles were obtained for all lignins. Data suggest that from 0 to 50% lignin (based on PBS weight), a direct proportionality between lignin addition and generated torque is observed, clearly indicating a progressive increase in viscosity. Above ca. 50% lignin, the slope of the torque changes, thus suggesting this concentration as a critical point where a decrease in compatibility between lignin and the PBS matrix occurs. This threshold can be regarded as a sort of "solubility limit" where above it, the blend is no longer homogeneous and torque rheometry starts to behave differently. Nevertheless, considering the high price of bio-PBS, ca. 4€/kg,[39] the addition of a high lignin content (up to 50%) with a much lower price of ca. 0.65−1 €/kg[40] can significantly reduce the final cost of the PBS-based composite.

Several concentrations of lignin were selected (i.e., 5, 10, 20, 30, 40, and 50 wt %) for producing the PBS-dealkaline lignin composites. As it can be observed in the top row of Figure S2, the coloration grade reflects the different concentrations of lignin (i.e., the darker the composite, the higher the

https://doi.org/10.1021/acsapm.3c02103
ACS Appl. Polym. Mater. 2024, 6, 1169−1181

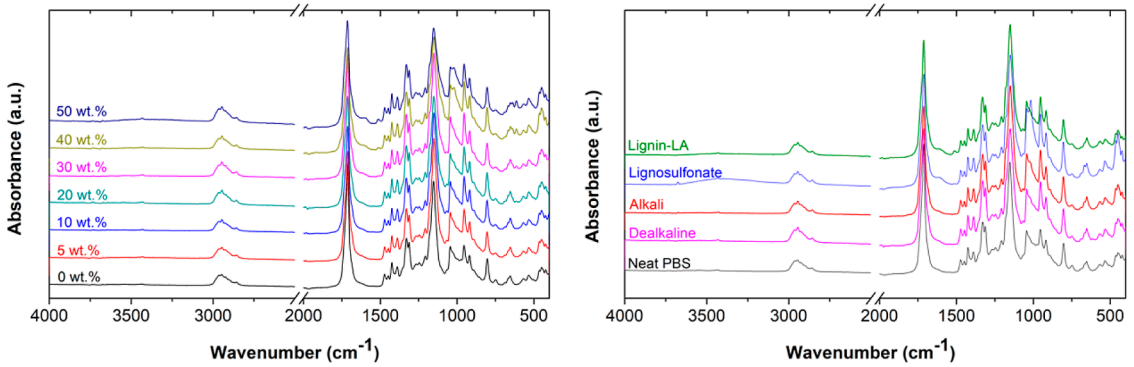

Figure 1. Normalized FTIR spectra of PBS-based composites with different concentrations of dealkaline lignin (left) and for different types of lignin (20 wt %) (right)

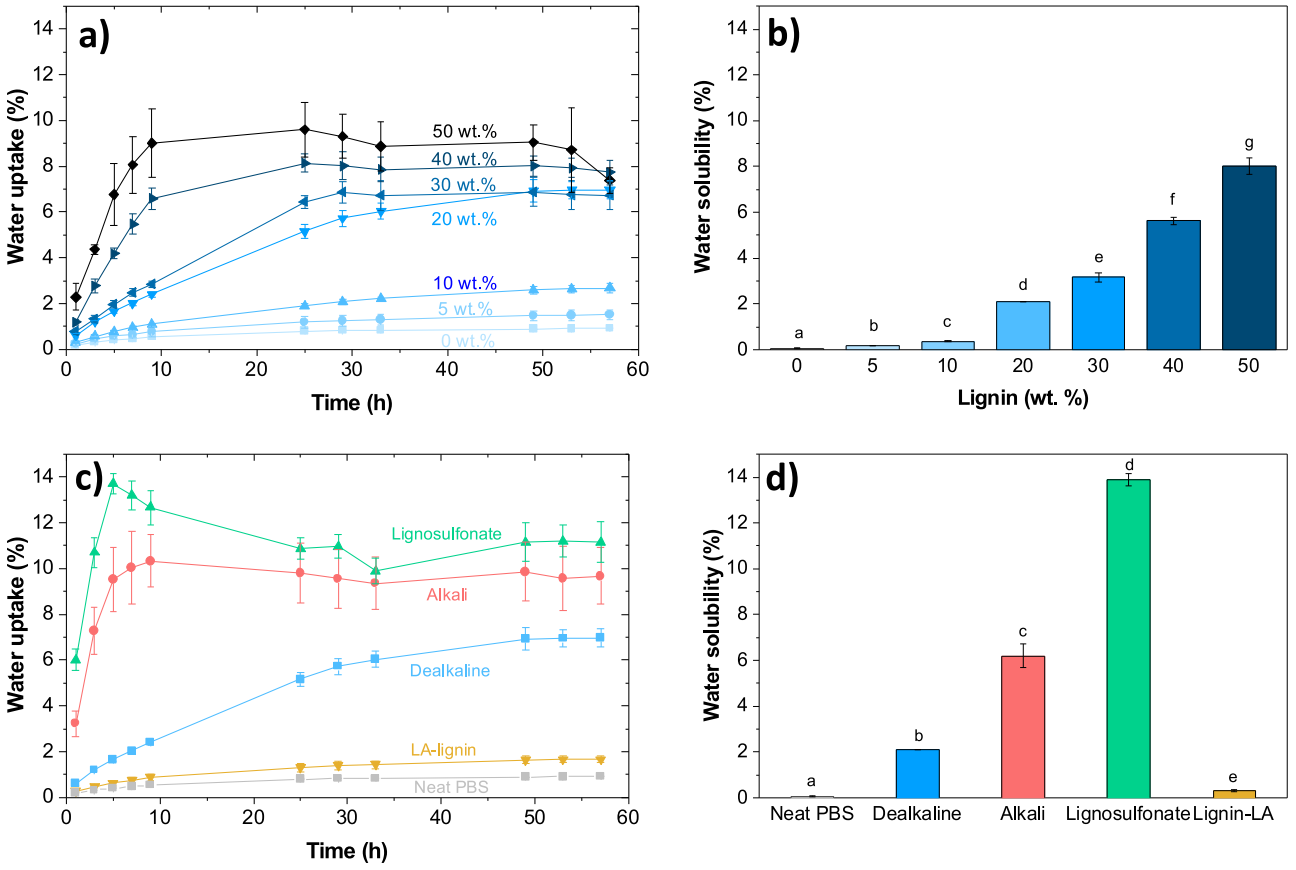

Figure 2. Water uptake (a,c) and water solubility (b,d) of PBS-based composites with different concentrations of dealkaline lignin (a,b) and different types of lignin (20 wt %) (c,d). Bars with different letters are significantly different from each other ($p < 0.05$).

concentration of lignin). Lignin particles typically present a polyhedral shape and an average size of less than 100 μm. Larger particles are observed for the LA-lignin samples (Figure S3). Composites with different types of lignin were also produced for a constant lignin concentration. Subtle changes in color are noticed among the different technical lignins (Figure S2, bottom row).

3.2. Functional Groups in the PBS/Lignin Composites. The FTIR spectra of neat PBS and PBS/lignin composites are shown in Figure 1. All the composites contain the same main bands assigned to the PBS (919 cm^{-1} due to the −C−OH bending of carboxylic acid groups, 1044 cm^{-1} due to the −O−C−C stretching vibration, 1153 cm^{-1} due to the −C−O−C stretching in ether linkages, 1712 cm^{-1} due to the C═O stretching vibration of ester groups, and 1330 and 2945 cm^{-1} due to the symmetric and asymmetric deformational vibrations of $-CH_2-$ groups[41]), but slight differences can be observed. With the increase of lignin concentration, a broadening of the band at 1018 cm^{-1} occurs due to the presence of more aromatic groups (C−H in-plane bending), primary alcohols (C−OH stretching), and C−O stretching of methyl ethers. A band at 1513 cm^{-1} also arises due to aromatic skeleton vibrations. Among the different lignins, slight changes can be observed particularly with lignosulfonate-based composite. Its spectrum exhibits a large band at 3050−3660 cm^{-1} and a broadening of the band at 1018 cm^{-1}. While the former is assigned to the OH stretching (protonated carboxylic and sulfonate groups), the latter is consistent with the S═O

https://doi.org/10.1021/acsapm.3c02103
ACS Appl. Polym. Mater. 2024, 6, 1169−1181

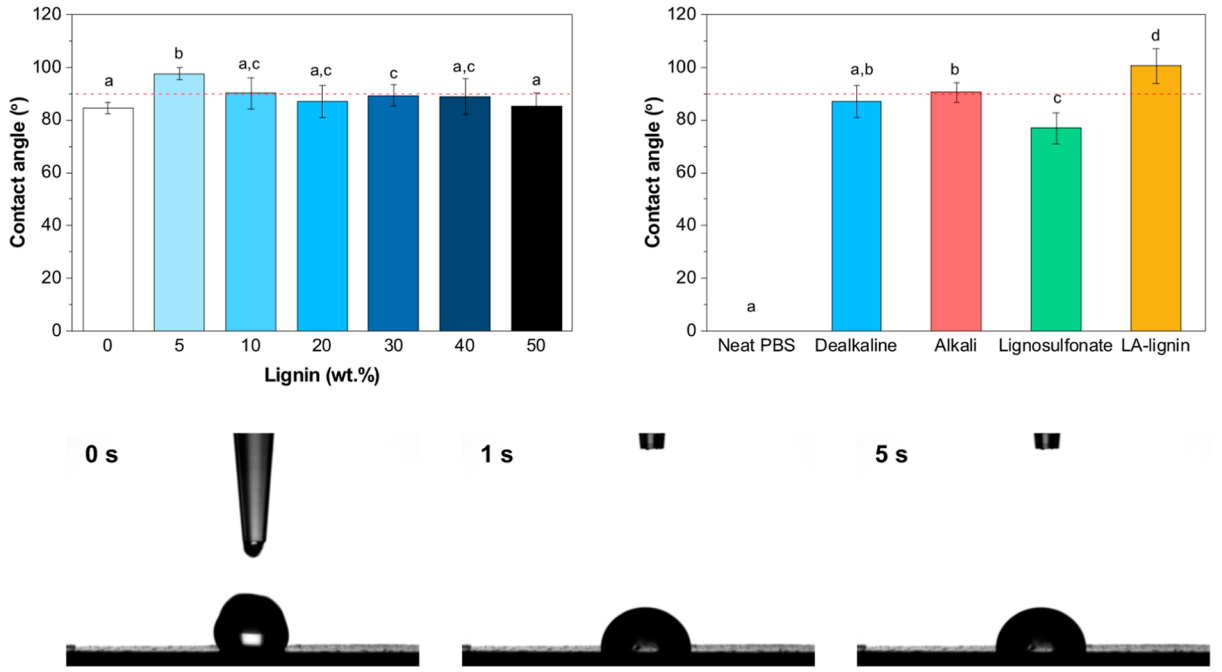

Figure 3. Contact angle of PBS with different concentrations of dealkaline lignin (left) and PBS-based composites with different types of lignin (20 wt %) (right). The red line denotes the transition from the hydrophilic behavior (contact angle < 90°) to the hydrophobic behavior (contact angle > 90°). Bars with different letters are significantly different from each other ($p < 0.05$). The pictures show the water drop on the surface of the composite with 5 wt % dealkaline lignin after 0, 1, and 5 s.

stretching. The spectra of all isolated lignins are shown in Figure S4.

3.3. Water Uptake and Solubility. In order to estimate the water uptake of the PBS-lignin composites, the percentage of absorbed water was measured as a function of time (Figure 2a,c). The rate of water uptake is generally faster during the first hours before reaching a plateau. In all the cases, the equilibrium in water uptake is reached after ca. 34 h. Moreover, a higher lignin content enhances the kinetics of water absorption and shifts the maximum of water uptake to higher values. This is possibly due to the presence of more microstructural defects (paths for water diffusion) and a more pronounced hydrophilic character of the composites with progressive lignin addition. It is also observed that the standard deviation generally increases for samples with higher lignin contents. The nonuniform distribution of lignin particles within the PBS matrix and/or possible particle aggregation may lead to areas in the composite enriched with such aggregates that are prone to absorb more water than other regions devoid of such structures, thereby resulting in a higher standard deviation.

The water uptake strikingly depends on the type of lignin used in the PBS-based composite (Figure 2c). A higher percentage of absorbed water was observed when using lignosulfonate and alkali lignins due to their superior hydrophilic nature. The most hydrophobic composites were obtained when using the extracted lignin from pine wood residues (LA-lignin) with a water uptake lower than ca. 2%, even after 57 h. It should be noticed that the water uptake of the composites follows the trend observed for the individual lignins: 1.9% for alkali lignin, 1.5% for dealkaline lignin, 2.2% for lignosulfonate, and 0.2% for LA-lignin after 24 h at room temperature. The values for water uptake and respective standard deviation can be found in Tables S1 and S2, respectively.

Similar trends were observed in the water solubility assays (Figure 2b), where significant differences were observed when varying the lignin concentration (i.e., increase of composite solubility with increasing lignin concentration in the PBS matrix).

Likewise, the type of lignin considerably affects the water solubility (Figure 2d), with the lignosulfonate-based composite presenting the highest value, ca. 14%. The LA-lignin based composite showed to be the least water-soluble thus corroborating the water uptake results and its less hydrophilic behavior. Among the technical lignins, it is also possible to observe that the higher the molecular weight, the lower the water solubility which is a combined feature of a decrease in the number of dissociating phenolic groups[42,43] and gradual loss of conformational entropy attributed for all polymers when the molecular weight is increasing.[44]

3.4. Hydrophobicity of PBS/Lignin Composites. The hydrophobicity of neat PBS and PBS/lignin composites was assessed by contact angle measurements (Figure 3). The neat PBS has a hydrophilic surface with a contact angle lower than 90°. A contact angle higher than 90° was obtained when using 5 wt % of dealkaline lignin, possibly suggesting a less hydrophilic surface, but surprisingly further addition of the polyphenol induces no significant differences between the resulting composites and neat PBS. This may suggest favorable interactions between the polyphenols and the PBS matrix, thus driving lignin away from the composite−air interface. Other possibility relies on the formation of a rougher surface upon lignin addition, thus presenting more lignin ends leaking onto the surface. Despite the high hydrophobic character of lignin, the surface defects favor wetting.[45] Compared to the various technical lignins, no significant differences were observed when using the dealkaline and alkali types. On the other hand, the use of lignosulfonate significantly decreases the contact angle, while the use of LA-lignin increases it. This can be rationalized

https://doi.org/10.1021/acsapm.3c02103
ACS Appl. Polym. Mater. 2024, 6, 1169−1181

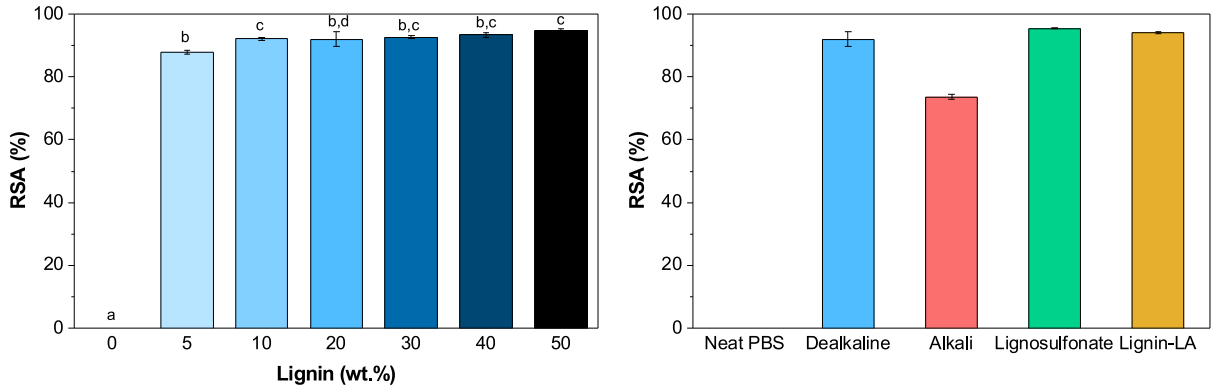

Figure 4. DPPH RSA of PBS with different concentrations of dealkaline lignin (left) and PBS-based composites with different types of lignin (20 wt %) (right). Bars with different letters are significantly different from each other ($p < 0.05$).

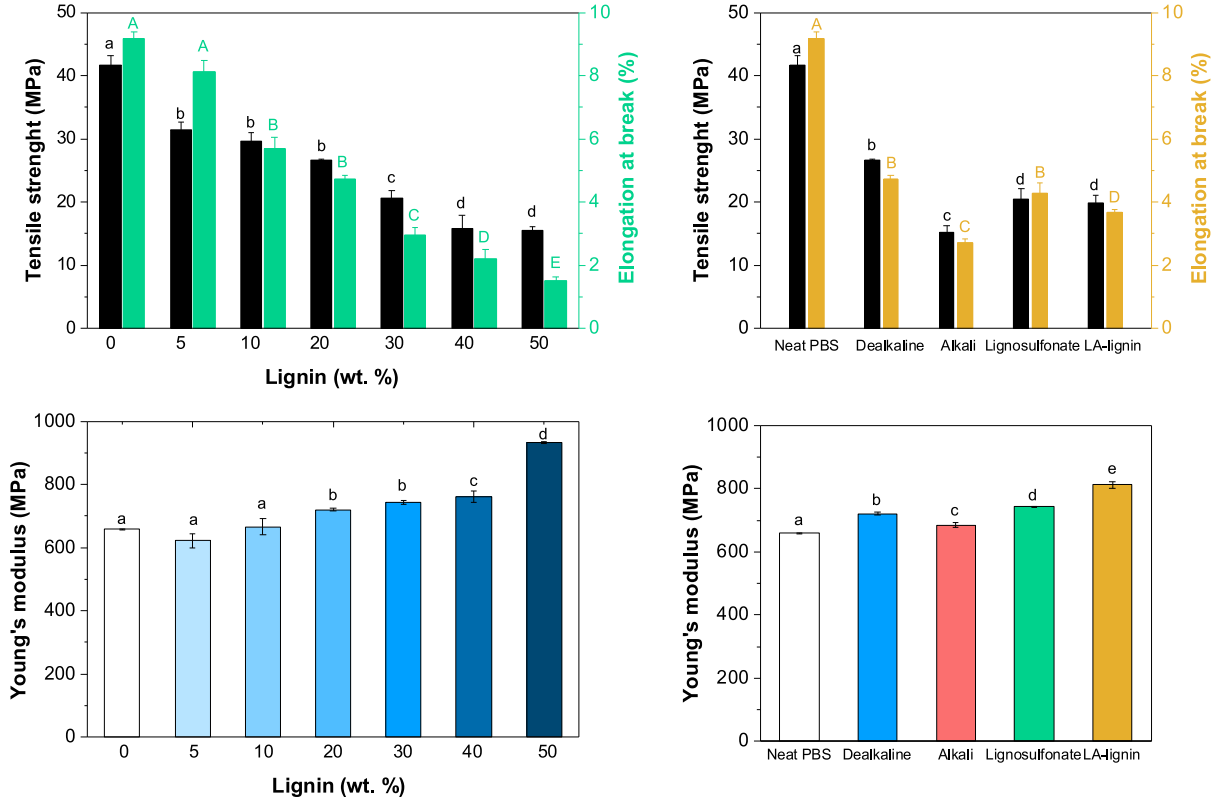

Figure 5. Mechanical properties of PBS with different concentrations of dealkaline lignin (left) and PBS-based composites with different types of lignin (20 wt %) (right). Bars with different letters are significantly different from each other ($p < 0.05$).

based on the relationship between roughness and wettability introduced by Wenzel.[46] When lignosulfonate is added, the material becomes more hydrophilic, presenting the lowest contact angle observed among the lignins used. At the same time, the contact angle in the PBS-lignosulfonate composite is the highest observed. Therefore, the material follows the trend predicted by the Wenzel equation as the hydrophilic properties of the native PBS were enhanced with the addition of lignosulfonate (which increases the roughness). On the other hand, the addition of LA-lignin to PBS decreases the roughness (in comparison to the native PBS). Such a decrease in roughness enhances the hydrophobicity of the composite, with the material reaching the highest contact angle. Overall, the roughness is expected to accentuate the pre-existing character of the material with respect to the contact angle which is predicted by the so-called Wenzel equation. These results are in perfect agreement with the water uptake and solubility assays, thus suggesting that the PBS-based composites with lignin extracted from pine residues are less hydrophilic than their counterparts. Besides, the composites with LA-lignin present the most homogeneous surface that, as discussed above, can also affect the contact angle.

3.5. Antioxidant Activity and Mechanical Performance of PBS/Lignin Composites. The antioxidant activities of neat PBS and PBS-lignin composites are shown in Figure 4. The neat PBS does not show any measurable RSA. On the other hand, the addition of 5 wt % of dealkaline lignin induces an RSA of 87.8 ± 0.7% which further increases to 92.1 ± 0.4% when the lignin amount raises to 10 wt %. Additional increment of lignin content in the composite has no significant

https://doi.org/10.1021/acsapm.3c02103
ACS Appl. Polym. Mater. 2024, 6, 1169−1181

effect on the measured RSA. The increase of the antioxidant activity of a PBS-based composite upon lignin addition has been reported in a related system where softwood kraft lignin (BioPiva 100) was used.[30] This effect has also been observed in other polymer matrices.[30,47−49] Among the different lignins, the alkali type presents the lowest antioxidant activity, ca. 74%. Nevertheless, it should be highlighted that no significant differences were observed among all of the remaining lignins, with all composites presenting the RSA above ca. 90%, thus demonstrating that these materials have interesting antioxidant properties.

Such antioxidant properties make these composites suitable for food packaging since they can extend the shelf life of food products by retarding/minimizing oxidative reactions.[50] Moreover, the high antioxidant features are also appealing for biomedical applications, such as in wound dressings,[51−53] because these composites can effectively reduce the concentration of reactive oxygen species and free radicals thus promoting faster wound healing.[30]

The mechanical features, namely, tensile strength, elongation at break, and Young's modulus, are represented in Figure 5. Neat PBS has a tensile strength of ca. 40 MPa. The addition of lignin significantly decreases the tensile strength. This property is further reduced with an increase in the lignin content. When 50 wt % of lignin is incorporated into PBS, the tensile strength is ca. 16 MPa.

The type of lignin is also observed to significantly affect the tensile strength. When comparing for the same amount of lignin (i.e., 20 wt %), dealkaline lignin confers the highest value, ca. 27 MPa, while the alkali lignin confers the poorest performance, ca. 15 MPa. This inferior behavior of the alkali type may be due to its more pronounced hydrophilic nature and therefore lower compatibility with the PBS matrix. On the other hand, the dealkaline lignin presents the highest M_w (Table S4), which could further contribute to an enhanced tensile strength of the formed composites. It should be mentioned that the elongation at the break follows the exact trend of the tensile strength (Figure 5, top row). Both the decrease in tensile strength and elongation at break agree with the previous reports using alkali lignin and lignosulfonate.[31,54] The decrease in tensile strength and elongation at break suggest a decrease in the interfacial adhesion between the lignin and PBS matrix.[31] A compilation of the tensile strength and elongation at break of PBS-lignin composites found in the literature can be found in Table S3. Overall, the mechanical results obtained in this work are comparable to other types of PBS-lignin composites. Nevertheless, upon an in-depth analysis of the works referenced in Table S3, it is important to note that such a comparison is not trivial, given the variations in the PBS type, the type and quantity of lignin, and the processing conditions. These factors strongly influence the properties of the composites, particularly the mechanical features. In fact, this challenge served as a strong motivation and driving force for conducting this study where all systems were processed under the same conditions and characterized with the same extended set of methods.

Regarding Young's modulus, no significant effects are observed up to 10 wt % lignin content. However, above this value, the increase in lignin concentration boosts the Young's modulus, indicating the enhancement in the rigidity of the composite. The lignin type is also observed to affect this parameter: the highest rigidity was obtained when using LA-lignin, ca. 812 MPa, while the alkaline lignin induces the formation of a softer material, ca. 685 MPa.

3.6. Thermal Behavior of PBS-Lignin Composites. The thermal stability of neat PBS and PBS-lignin composites was assessed by thermogravimetric analysis (TGA). The thermograms are represented in Figure S5, while the most relevant thermal stability parameters (i.e., temperature at 5, 10, and 50% weight loss, maximum decomposition temperature, and residue at 600 °C) are summarized in Table 1. The addition of small amounts of lignin (ca. 5 wt %) improves the thermal stability since the decomposition temperatures (T_d) for 5, 10, and 50% weight loss are observed to increase. Above 5 wt % lignin, all the composites present lower decomposition temperatures, for 5 and 10% weight loss. At 50% weight loss, there was no significant variation of decomposition temperature, being around 377 to 380 °C. The maximum decomposition temperature, T_{max}, is 387 °C for neat PBS, and all the composites present a slight shift, ranging between 379 and 385 °C. The residue at 600 °C increases with the increase of lignin concentration, from 3.6 to 25.1, using 5 and 50 wt % dealkaline lignin, respectively. This agrees with related studies where, for instance, when using Arboform F 45 as lignin, the authors have observed that the residue formed at 600 °C increases with the lignin content, most likely due the highly condensed aromatic structures.[29]

Table 1. Thermal Degradation Properties of PBS-Lignin Composites

type of lignin	lignin (wt %)	T_d (5%)	T_d (10%)	T_d (50%)	T_{max} (°C)	residue at 600 °C (%)
*	0	324	340	377	387	0.9
dealkaline	5	326	344	380	385	3.6
	10	314	340	379	382	8.0
	20	300	335	379	382	13.4
	30	261	318	378	382	17.1
	40	230	302	377	379	21.7
	50	202	275	377	380	25.1
alkali	20	272	321	378	385	12.2
lignosulfonate	20	240	296	375	382	11.2
LA-lignin	20	288	339	383	386	6.4

The type of lignin also affects the residue at 600 °C, being the highest value obtained when using dealkaline lignin, i.e., 13.4% and the lowest value when using LA-lignin, 6.4%. The residue amount follows the M_w trend (see Table S4), and this might be related to the formation of more stable and cross-linked structures that higher M_w lignins may provide.

3.7. Morphology of Composites: SEM and AFM. The PBS-lignin composites were evaluated regarding their morphology by SEM and AFM (Figure 6). The SEM images demonstrate that the biocomposite containing 5 wt % dealkaline lignin (Figure 6B) has a morphology similar to neat PBS (Figure 6A). However, further addition of lignin (Figure 6C,D) induces the formation of a more heterogeneous material with the presence of small lignin particles. The SEM data suggest that the PBS matrix and lignins are mostly compatible. Depending on the lignin type used, the degree of homogeneity changes and this is, in fact, perceptible in the SEM images. As mentioned, increasing the lignin content makes the system progressively less homogeneous.

In the PBS-alkali lignin composite (Figure 6E), some pits are observed due to the removal of lignin particles when the

https://doi.org/10.1021/acsapm.3c02103
ACS Appl. Polym. Mater. 2024, 6, 1169−1181

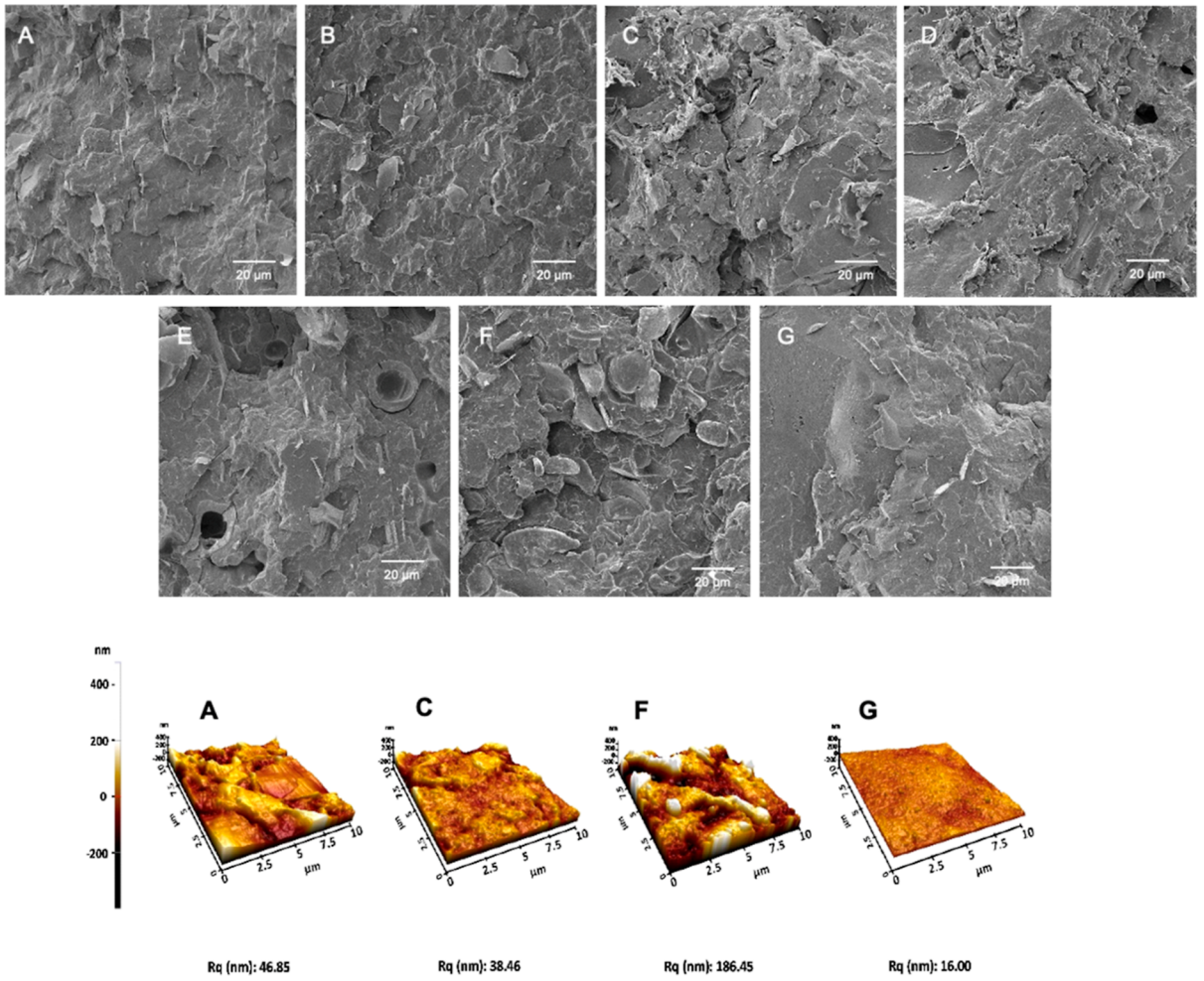

Figure 6. (Top) SEM images of fractured surfaces and bottom) AFM three-dimensional (3D) images of neat PBS (A), and PBS-based composites with 5 (B), 20 (C), and 50 wt % (D) dealkaline lignin, 20 wt % alkali lignin (E), 20 wt % lignosulfonate (F), and 20 wt % LA-lignin (G). All scale-bars represent 20 μm.

composite was fractured. Again, this might suggest the lower compatibility of this type of lignin with the PBS matrix, which supports the poorer mechanical performance (tensile strength and elongation at break) shown in Figure 5. A highly heterogeneous mixture with big lignin particles is observed when using lignosulfonate (Figure 6F). On the other hand, the composites with LA-lignin present a more homogeneous and smoother structure (Figure 6G), which might suggest an improved incorporation of LA-lignin into the PBS matrix. The NMR analysis of LA-lignin suggests the occurrence of esterification reactions on the aliphatic OH groups with levulinic acid.[34] In fact, Liu et al. have shown that it is possible to obtain esterified lignins using organic acids as a solvent and reagent at high temperatures.[55] Therefore, it is reasonable to assume that esterification enhances the compatibility of lignin with the PBS matrix.

From the AFM measurements, it is possible to confirm that the PBS/LA-lignin composite shows the lowest roughness (lower Rq value), while neat PBS and PBS-dealkaline lignin present similar roughness. Moreover, the PBS-lignosulfonate composite renders the most heterogeneous structure with the highest roughness, which is in good agreement with the SEM data.

3.8. Bacteria–Composite Interaction. Bacterial adherence to the PBS-based biocomposites was evaluated using the Gram-negative *E. coli* and the Gram-positive *S. aureus*. Lignin has been reported to possess antibacterial properties, mainly in Gram-positive bacteria, having almost no effect on Gram-negative, namely, *E. coli*.[30] Figure 7 shows that bacterial adhesion (assessed as colony forming units, cfu) of *E. coli* generally increases in the composites, with respect to neat PBS (without lignin). On the other hand, PBS containing alkali or dealkaline lignin promotes a decrease in the number of *S.*

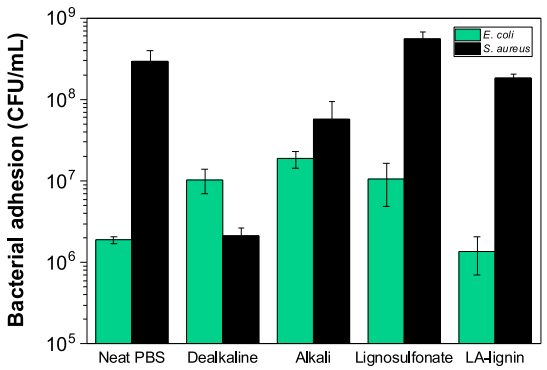

Figure 7. Bacterial adhesion of *E. coli* and *S. aureus* on the different composites is given as cfu mL^{-1}.

https://doi.org/10.1021/acsapm.3c02103
ACS Appl. Polym. Mater. 2024, 6, 1169−1181

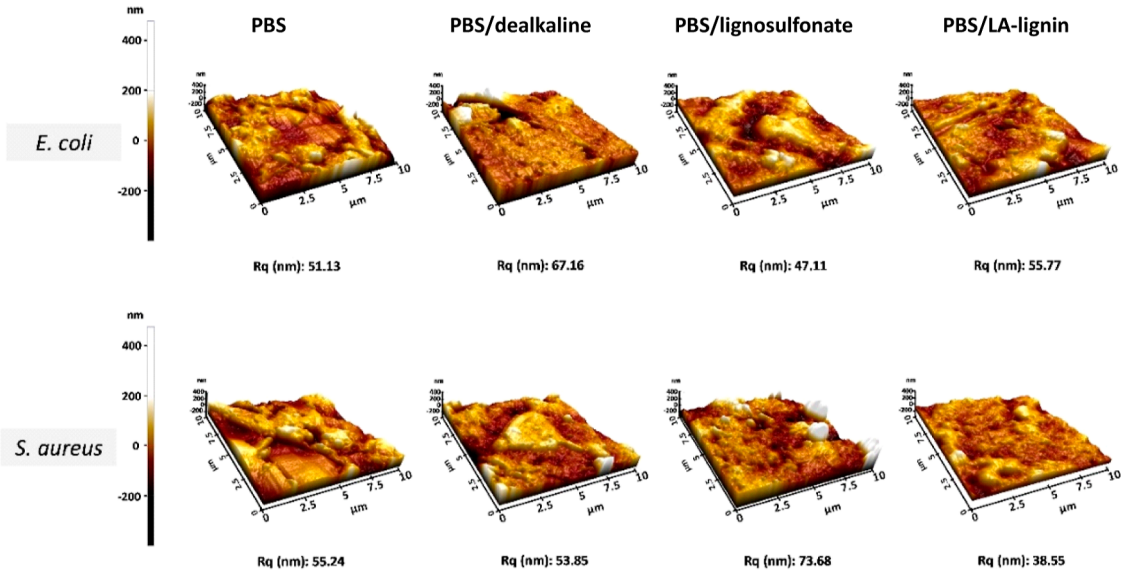

Figure 8. AFM 3D image of the PBS-based composites with 20 wt % different types of lignin after 24 h immersion in a bacterial culture of *E. coli* or *S. aureus*.

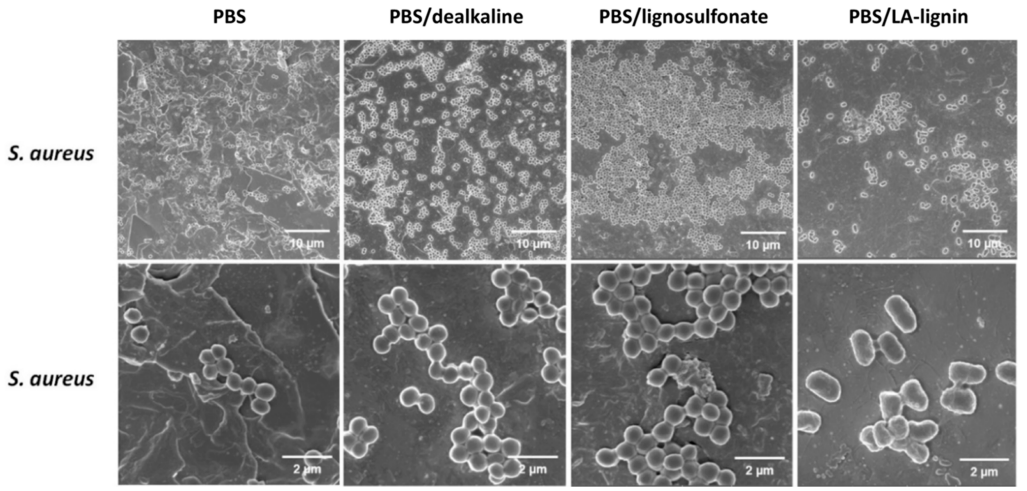

Figure 9. SEM images of PBS-based composites with bacterial cells (*S. aureus*) at two different magnifications. Scale-bars 10 mm (top row), 2 mm (bottom row)

aureus cells; PBS-alkali lignin composites induce a slight decrease, close to 1 log cfus reduction, while PBS-dealkaline lignin demonstrates to be the most effective composite with a 2 log cfus reduction in the number of *S. aureus* attached.

Such differences could be related to several factors, such as the composite hydrophilicity/hydrophobicity balance, lignin molecular weight, molecular composition in the bacterial cell wall, etc. Apart from the PBS/LA-lignin composite, all systems manifest a slightly pronounced hydrophilic behavior, and thus this might explain the higher *E. coli* adhesion to alkali, dealkaline, and lignosulfonate-based composites. It should be recalled that bacteria are generally regarded as hydrophilic, and *E. coli* is a good example of such behavior, presenting rather low contact angles.[56−58] On the other hand, the PBS/LA-lignin composite presents a more hydrophobic behavior, and thus it is less prone to interact with hydrophilic *E. coli*.

It has also been reported that *S. aureus* adhesion to different surfaces occurs via by thermally fluctuating cell wall macromolecules whose behavior apparently depends on the nature of the substrate.[59] On the contrary to *E. coli*, it has been shown by single-cell force spectroscopy that adhesion of *S. aureus* to hydrophobic surfaces is about 1 order of magnitude greater than that to hydrophilic substrates.[60,61] Surprisingly, that seems not to be the case here since the cfu of *S. aureus* in neat PBS is higher than that for *E. coli*.

According to the suppliers, the dealkaline lignin is obtained from the lignosulfonate lignin after a series of chemical modifications, such as partial desulfonation, oxidation, hydrolysis, and demethylation. The lower adhesion of Gram-positive bacteria to materials composed of this type of lignin can be related to the outer membrane composition. Gram-positive bacteria cell walls are much richer in phospholipids and lipoproteins than Gram-negative, which might enhance the permeability of less hydrophilic compounds, such as dealkaline lignin.[62]

On the other hand, the increase in bacterial adhesion shown for PBS-lignosulfonate composites could be related to the lignosulfonate ability of precipitating proteins.[63]

3.9. Bacterial Effect on the Roughness and Structure of the Composites. The AFM assays also show an increase in

https://doi.org/10.1021/acsapm.3c02103
ACS Appl. Polym. Mater. 2024, 6, 1169−1181

the roughness of all PBS-lignin composites (supporting bacteria adhesion), except for the PBS-lignosulfonate composite, where there was a decrease (Figure 8A,B). The former observation might be due to the deposition of bacterial cells. The *E. coli* radius can vary between 0.5 and 0.8 μm, while *S. aureus* radius can vary between 0.5 and 1.5 μm.[64,65] The height of the analyzed composite layer is approximately 800 nm (scale bar); this way, the smoothest surfaces should present an increase in roughness when bacteria attach. With respect to the roughest composite, PBS-lignosulfonate, the characteristic valleys should be deep enough to be filled with bacteria, thus reducing the composite roughness. Moreover, the surface with a higher affinity to proteins allowing its precipitation should allow for an easier bacterial attachment and bacterial survivability chances.[66,67] These AFM observations are supported by the SEM of composites with *S. aureus* bacteria (Figure 9) where enhanced adhesion of cells in the roughest composite (PBS-lignosulfonate) induces the apparent formation of a smoother bacteria film.

Overall, it should be highlighted that the PBS-LA lignin composite shows a similar effect in both Gram-negative and Gram-positive bacterial strains by slightly reducing bacterial attachment. This composite also showed to be the least water-soluble, most hydrophobic, and with the lowest roughness.

The bacterial adhesion effect on the composite structure was also evaluated by XRD (Figure S6). The diffractogram peaks for PBS-lignin composites are typical of the neat PBS structure. The characteristic peaks for PBS located at the diffraction angles (2θ) ca. 19.6, 21.9, 22.8, and 28.8° are observed; which correspond to the diffraction of (020), (021), (110), and (111) crystallographic plane reflections, respectively.[68,69] The XRD patterns of the composites adsorbed with bacteria show slight differences among the different types of lignin used, mainly regarding a minor intensity reduction of the characteristic diffraction peaks from PBS at 19.6, 21.9, and 22.8°. In addition, the introduction of lignin (amorphous) in the PBS matrix has also caused considerable reduction in the intensity of the diffraction peak (111) located at $2\theta \sim 28.8°$. As mentioned, the addition of bacteria has no major effect on the intensity or position of the characteristic peaks of the neat PBS and its lignin-based composites. However, an extra peak at ca. 32.5° is observed when *S. aureus* cells were added to the PBS-dealkaline lignin composite and when both *S. aureus* and *E. coli* strains were added to PBS-LA-lignin composite. Interestingly, this agrees with the data regarding bacterial adhesion on the PBS-dealkaline lignin and PBS-LA-lignin composites that were the most effective in reducing the number of bacteria attached (bacterial adhesion with positive log cfus). This correlation may be used to monitor the antibacterial properties of the PBS-lignin composites against various bacterial strains. Nevertheless, the validation of such a hypothesis and its underlying mechanism requires further investigation.

4. CONCLUSIONS

In this work, several biobased composites using PBS as the biodegradable polymer matrix were successfully developed and characterized, using different types of technical lignins and a type of lignin extracted from pine residues. A maximum content of about 50% lignin (based on PBS weight) in the PBS composite was found by torque rheometry. Above this critical value, the PBS-lignin compatibility might be compromised. The water uptake and water solubility increase with the lignin content in the composites, which is presumably related to the existence of structural defects in the PBS matrix which facilitates water diffusion. These structural defects are probed by the AFM and SEM data and arise from the composite heterogeneity. The diffusion and solubility of lignin is enhanced for the most hydrophilic lignin (lignosulfonate), while the LA-lignin presents the lowest aqueous solubility, most likely due to favorable interactions with the PBS matrix. These favorable interactions between the LA-lignin and PBS matrix are suggested to be responsible for the enhanced Young's modulus and thermal properties observed in LA-lignin/PBS composites. In addition, the higher compatibility between the LA-lignin and PBS matrix also manifests itself in the formation of highly homogeneous films, as probed by SEM and AFM, where smoother surfaces with low roughness are observed. Finally, it should be mentioned that, regardless of the type of lignin used, all composites display remarkable high antioxidant activity, which is anticipated for polyphenol-based materials. The PBS dealkaline lignin composites were found to present the highest bacterial antiadhesion effect against *S. aureus* by reducing bacterial attachment by 2 log/cfus with respect to neat PBS. Interestingly, the PBS/LA-lignin composites show a similar antiadhesion effect on *E. coli* and *S. aureus*, thus making this composite highly promising for future material development targeting simultaneous activity toward Gram-positive and Gram-negative bacteria. It is believed that such enhanced activity toward both types of bacteria is due to the special properties of this type of lignin (LA-Lignin), in particular the higher content in carbonyl groups. Nevertheless, further studies are needed to clearly elucidate the mechanisms driving the versatility of LA-lignin.

■ ASSOCIATED CONTENT

Supporting Information

The Supporting Information is available free of charge at https://pubs.acs.org/doi/10.1021/acsapm.3c02103.

Figures: Equilibrium torque as a function of lignin content; photographs of PBS-lignin composites; optical microscopy images of lignin powder; FTIR of lignins; thermograms of the composites; XRD of composites with and without bacteria. Tables: water uptake and standard deviation; mechanical features of PBS-Lignin composites; molecular weight averages of lignins used (PDF)

■ AUTHOR INFORMATION

Corresponding Author

Elodie Melro − *University of Coimbra, Department of Chemistry, CQC, Rua Larga, Coimbra 3004-535, Portugal; Science 351—Disruptive & Sustainable R&D Innovations, Instituto Pedro Nunes, Ed. C, Coimbra 3030-199, Portugal;* orcid.org/0000-0003-1401-7164; Email: elodie.melro@uc.pt

Authors

Hugo Duarte − *MED-Mediterranean Institute for Agriculture, Environment and Development, CHANGE−Global Change and Sustainability Institute, Faculdade de Ciências e Tecnologia, Universidade do Algarve, 8005-139 Faro, Portugal;* orcid.org/0000-0001-6461-3541

Alireza Eivazi − *FSCN Research Center, Surface and Colloid Engineering, Mid Sweden University, SE-851 70 Sundsvall, Sweden;* orcid.org/0000-0001-6270-2970

https://doi.org/10.1021/acsapm.3c02103
ACS Appl. Polym. Mater. 2024, 6, 1169−1181

Carolina Costa − *FSCN Research Center, Surface and Colloid Engineering, Mid Sweden University, SE-851 70 Sundsvall, Sweden*

Maria L. Faleiro − *Faculdade de Ciências e Tecnologia, C8, Campus de Gambelas, Universidade do Algarve, Faro 8005-139, Portugal; Algarve Biomedical Center, Research Institute, Faro 8005-139, Portugal; Champalimaud Research Program, Champalimaud Centre for the Unknown, Lisbon 1400-038, Portugal*

Ana M. Rosa da Costa − *Center for Electronics, Optoelectronics and Telecommunications (CEOT), Faculdade de Ciências e Tecnologia, Universidade do Algarve, Faro 8005-139, Portugal*

Filipe E. Antunes − *University of Coimbra, Department of Chemistry, CQC, Rua Larga, Coimbra 3004-535, Portugal; Science 351—Disruptive & Sustainable R&D Innovations, Instituto Pedro Nunes, Ed. C, Coimbra 3030-199, Portugal*

Artur J. M. Valente − *University of Coimbra, Department of Chemistry, CQC, Rua Larga, Coimbra 3004-535, Portugal;* orcid.org/0000-0002-4612-7686

Anabela Romano − *MED-Mediterranean Institute for Agriculture, Environment and Development, CHANGE−Global Change and Sustainability Institute, Faculdade de Ciências e Tecnologia, Universidade do Algarve, 8005-139 Faro, Portugal*

Magnus Norgren − *FSCN Research Center, Surface and Colloid Engineering, Mid Sweden University, SE-851 70 Sundsvall, Sweden;* orcid.org/0000-0003-3407-7973

Bruno Medronho − *MED-Mediterranean Institute for Agriculture, Environment and Development, CHANGE−Global Change and Sustainability Institute, Faculdade de Ciências e Tecnologia, Universidade do Algarve, 8005-139 Faro, Portugal; FSCN Research Center, Surface and Colloid Engineering, Mid Sweden University, SE-851 70 Sundsvall, Sweden;* orcid.org/0000-0003-0972-1739

Complete contact information is available at: https://pubs.acs.org/10.1021/acsapm.3c02103

Funding

This work was supported by funding from the Portuguese Foundation for Science and Technology (FCT) through the projects PTDC/AGR-TEC/4814/2014, ALG-01-0145-FEDER-030619 • POCI-01-0145-FEDER-030619 - PTDC/ASP-SIL/30619/2017, UIDB/05183/2020 and the researcher grant CEECIND/01014/2018. Elodie Melro is grateful for the PhD grant (SFRH/BD/132835/2017) from FCT. The CQC is supported by FCT through the project projects UID/QUI/00313/2020 and COMPETE.

Notes

The authors declare no competing financial interest.

■ ABBREVIATIONS

DPPH, 2-diphenyl-1-picrylhydrazyl; FE-SEM, field emission scanning electron microscopy; FTIR, Fourier transform infrared spectroscopy; LA-lignin, lignin extracted from pine wood using levulinic acid; LDPE, low-density polyethylene; Mn, number-average molecular weight; Mp, molecular weight at the peak; M_w, weight-average molecular weight; PBS, poly(butylene succinate); PE, polyethylene; PP, polypropylene; RSA, radical scavenging activity; SEC, size exclusion chromatography; SEM, scanning electron microscopy; T_d, decomposition temperature; TGA, thermogravimetric analysis; T_{max}, maximum decomposition temperature; W_a, water absorption capacity; XRD, X-ray diffraction

■ REFERENCES

(1) Global Plastics Flow 2018. https://www.euromap.org/media/news/Global_Plastics_Flow_Summary_Oct_2019.pdf (accessed June 28, 2023).

(2) Kabir, E.; Kaur, R.; Lee, J.; Kim, K. H.; Kwon, E. E. Prospects of Biopolymer Technology as an Alternative Option for Non-Degradable Plastics and Sustainable Management of Plastic Wastes. *J. Clean. Prod.* **2020**, *258*, 120536.

(3) Haider, T. P.; Völker, C.; Kramm, J.; Landfester, K.; Wurm, F. R. Plastics of the Future? The Impact of Biodegradable Polymers on the Environment and on Society. *Angew. Chem., Int. Ed.* **2019**, *58* (1), 50−62.

(4) Huang, Z.; Qian, L.; Yin, Q.; Yu, N.; Liu, T.; Tian, D. Biodegradability Studies of Poly(Butylene Succinate) Composites Filled with Sugarcane Rind Fiber. *Polym. Test.* **2018**, *66* (June 2017), 319−326.

(5) Aliotta, L.; Seggiani, M.; Lazzeri, A.; Gigante, V.; Cinelli, P. A Brief Review of Poly (Butylene Succinate)(PBS) and Its Main Copolymers: Synthesis, Blends, Composites, Biodegradability, and Applications. *Polymers* **2022**, *14* (4), 844.

(6) Chrissafis, K.; Paraskevopoulos, K. M.; Bikiaris, D. N. Thermal Degradation Mechanism of Poly(Ethylene Succinate) and Poly(Butylene Succinate): Comparative Study. *Thermochim. Acta* **2005**, *435* (2), 142−150.

(7) Zhang, Y.; Yu, C.; Chu, P. K.; Lv, F.; Zhang, C.; Ji, J.; Zhang, R.; Wang, H. Mechanical and Thermal Properties of Basalt Fiber Reinforced Poly(Butylene Succinate) Composites. *Mater. Chem. Phys.* **2012**, *133* (2−3), 845−849.

(8) Liu, L.; Yu, J.; Cheng, L.; Qu, W. Mechanical Properties of Poly(Butylene Succinate) (PBS) Biocomposites Reinforced with Surface Modified Jute Fibre. *Composites, Part A* **2009**, *40* (5), 669−674.

(9) Siracusa, V.; Lotti, N.; Munari, A.; Dalla Rosa, M. Poly(Butylene Succinate) and Poly(Butylene Succinate-Co-Adipate) for Food Packaging Applications: Gas Barrier Properties after Stressed Treatments. *Polym. Degrad. Stab.* **2015**, *119*, 35−45.

(10) Vytejčková, S.; Vápenka, L.; Hradecký, J.; Dobiáš, J.; Hajšlová, J.; Loriot, C.; Vannini, L.; Poustka, J. Testing of Polybutylene Succinate Based Films for Poultry Meat Packaging. *Polym. Test.* **2017**, *60*, 357−364.

(11) Ayu, R. S.; Khalina, A.; Harmaen, A. S.; Zaman, K.; Mohd Nurrazi, N.; Isma, T.; Lee, C. H. Effect of Empty Fruit Brunch Reinforcement in PolyButylene-Succinate/Modified Tapioca Starch Blend for Agricultural Mulch Films. *Sci. Rep.* **2020**, *10* (1), 1166.

(12) Gigli, M.; Fabbri, M.; Lotti, N.; Gamberini, R.; Rimini, B.; Munari, A. Poly(butylene succinate)-based polyesters for biomedical applications: A review. *Eur. Polym. J.* **2016**, *75*, 431−460.

(13) Joy, J.; Jose, C.; Yu, X.; Mathew, L.; Thomas, S.; Pilla, S. The Influence of Nanocellulosic Fiber, Extracted from Helicteres Isora, on Thermal, Wetting and Viscoelastic Properties of Poly(Butylene Succinate) Composites. *Cellulose* **2017**, *24* (10), 4313−4323.

(14) Hu, C.; Bourbigot, S.; Delaunay, T.; Collinet, M.; Marcille, S.; Fontaine, G. Synthesis of Isosorbide Based Flame Retardants: Application for Polybutylene Succinate. *Polym. Degrad. Stab.* **2019**, *164*, 9−17.

(15) Liu, H. Y.; Chen, F. Q.; Guo, R. B.; Zhang, G.; Qu, J. Effect of Compatibilizer on the Properties of PBS/Lignin Composites Prepared via a Vane Extruder. *J. Polym. Eng.* **2015**, *35* (9), 829−837.

(16) Mochane, M. J.; Magagula, S. I.; Sefadi, J. S.; Mokhena, T. C. A Review on Green Composites Based on Natural Fiber-Reinforced Polybutylene Succinate (PBS). *Polymers* **2021**, *13* (8), 1200.

(17) Rai, P.; Mehrotra, S.; Priya, S.; Gnansounou, E.; Sharma, S. K. Recent Advances in the Sustainable Design and Applications of Biodegradable Polymers. *Bioresour. Technol.* **2021**, *325*, 124739.

(18) Azadi, P.; Inderwildi, O. R.; Farnood, R.; King, D. A. Liquid Fuels, Hydrogen and Chemicals from Lignin: A Critical Review. *Renew. Sustain. Energy Rev.* **2013**, *21*, 506−523.
(19) Vishtal, A.; Kraslawski, A. Challenges in Industrial Applications of Technical Lignins. *Bioresources* **2011**, *6* (3), 3547−3568.
(20) Stanisz, M.; Klapiszewski, Ł.; Collins, M.; Jesionowski, T. Recent Progress in Biomedical and Biotechnological Applications of Lignin-Based Spherical Nano-and Microstructures: A Comprehensive Review. *Mater. Today Chem.* **2022**, *26*, 101198.
(21) Melro, E.; Filipe, A.; Sousa, D.; Medronho, B.; Romano, A. Revisiting Lignin: A Tour through Its Structural Features, Characterization Methods and Applications. *New J. Chem.* **2021**, *45* (16), 6986−7013.
(22) Chiani, E.; Beaucamp, A.; Hamzeh, Y.; Azadfallah, M.; Thanusha, A. V.; Collins, M. N. Synthesis and Characterization of Gelatin/Lignin Hydrogels as Quick Release Drug Carriers for Ribavirin. *Int. J. Biol. Macromol.* **2023**, *224*, 1196−1205.
(23) Culebras, M.; Pishnamazi, M.; Walker, G. M.; Collins, M. N. Facile Tailoring of Structures for Controlled Release of Paracetamol from Sustainable Lignin Derived Platforms. *Molecules* **2021**, *26* (6), 1593.
(24) Beaucamp, A.; Muddasar, M.; Crawford, T.; Collins, M. N.; Culebras, M. Sustainable Lignin Precursors for Tailored Porous Carbon-Based Supercapacitor Electrodes. *Int. J. Biol. Macromol.* **2022**, *221*, 1142−1149.
(25) Jędrzejczak, P.; Collins, M. N.; Jesionowski, T.; Klapiszewski, Ł. The Role of Lignin and Lignin-Based Materials in Sustainable Construction-a Comprehensive Review. *Int. J. Biol. Macromol.* **2021**, *187*, 624−650.
(26) Liu, L.; Huang, G.; Song, P.; Yu, Y.; Fu, S. Converting Industrial Alkali Lignin to Biobased Functional Additives for Improving Fire Behavior and Smoke Suppression of Polybutylene Succinate. *ACS Sustain. Chem. Eng.* **2016**, *4* (9), 4732−4742.
(27) Ferry, L.; Dorez, G.; Taguet, A.; Otazaghine, B.; Lopez-Cuesta, J. M. Chemical Modification of Lignin by Phosphorus Molecules to Improve the Fire Behavior of Polybutylene Succinate. *Polym. Degrad. Stab.* **2015**, *113*, 135−143.
(28) Zhang, Y.; Zhou, S.; Fang, X.; Zhou, X.; Wang, J.; Bai, F.; Peng, S. Renewable and Flexible UV-Blocking Film from Poly(Butylene Succinate) and Lignin. *Eur. Polym. J.* **2019**, *116* (April), 265−274.
(29) Sahoo, S.; Misra, M.; Mohanty, A. K. Enhanced Properties of Lignin-Based Biodegradable Polymer Composites Using Injection Moulding Process. *Composites, Part A* **2011**, *42*, 1710−1718.
(30) Domínguez-Robles, J.; Larrañeta, E.; Fong, M. L.; Martin, N. K.; Irwin, N. J.; Mutjé, P.; Tarrés, Q.; Delgado-Aguilar, M. Lignin/Poly(Butylene Succinate) Composites with Antioxidant and Antibacterial Properties for Potential Biomedical Applications. *Int. J. Biol. Macromol.* **2020**, *145*, 92−99.
(31) Fan, D.; Chang, P. R.; Lin, N.; Yu, J.; Huang, J. Structure and Properties of Alkaline Lignin-Filled Poly(Butylene Succinate) Plastics. *Iran. Polym. J.* **2011**, *20*, 3−14.
(32) Magalhães, S.; Filipe, A.; Melro, E.; Fernandes, C.; Vitorino, C.; Alves, L.; Romano, A.; Rasteiro, M. G.; Medronho, B. Lignin Extraction from Waste Pine Sawdust Using a Biomass Derived Binary Solvent System. *Polymers* **2021**, *13* (7), 1090.
(33) Melro, E.; Filipe, A.; Valente, A. J. M.; Antunes, F. E.; Romano, A.; Norgren, M.; Medronho, B. Levulinic Acid: A Novel Sustainable Solvent for Lignin Dissolution. *Int. J. Biol. Macromol.* **2020**, *164*, 3454−3461.
(34) Melro, E.; Riddell, A.; Bernin, D.; da Costa, A. M. R.; Valente, A. J. M.; Antunes, F. E.; Romano, A.; Norgren, M.; Medronho, B. Levulinic Acid-Based "Green" Solvents for Lignocellulose Fractionation: On the Superior Extraction Yield and Selectivity toward Lignin. *Biomacromolecules* **2023**, *24* (7), 3094−3104.
(35) Standard, A. *D570−98: Standard Test Method for Water Absorption of Plastics*; American Society for Testing and Materials: New York, 1998.
(36) Alzagameem, A.; Klein, S. E.; Bergs, M.; Do, X. T.; Korte, I.; Dohlen, S.; Hüwe, C.; Kreyenschmidt, J.; Kamm, B.; Larkins, M.; Schulze, M. Antimicrobial Activity of Lignin and Lignin-Derived Cellulose and Chitosan Composites against Selected Pathogenic and Spoilage Microorganisms. *Polymers* **2019**, *11* (4), 670.
(37) International, A. *ASTM D638−14, Standard Test Method for Tensile Properties of Plastics*; ASTM International, 2015.
(38) Thomas, P.; Sekhar, A. C.; Upreti, R.; Mujawar, M. M.; Pasha, S. S. Optimization of Single Plate-Serial Dilution Spotting (SP-SDS) with Sample Anchoring as an Assured Method for Bacterial and Yeast Cfu Enumeration and Single Colony Isolation from Diverse Samples. *Biotechnol. Rep.* **2015**, *8*, 45−55.
(39) Van den Oever, M.; Molenveld, K.; van der Zee, M.; Bos, H. *Bio-Based and Biodegradable Plastics: Facts and Figures: Focus on Food Packaging in the Netherlands*; Report 1722; Wageningen Food & Biobased Research, 2017, 1−67.
(40) European Commission Papers: The Lignin Briefing. https://bioplasticsnews.com/2018/08/10/european-commission-lignin/ (accessed June 06, 2023).
(41) Phua, Y. J.; Chow, W. S.; Mohd Ishak, Z. A. Reactive Processing of Maleic Anhydride-Grafted Poly (Butylene Succinate) and the Compatibilizing Effect on Poly (Butylene Succinate) Nanocomposites. *Express Polym. Lett.* **2013**, *7* (4), 340−354.
(42) Norgren, M.; Lindström, B. Dissociation of Phenolic Groups in Kraft Lignin at Elevated Temperatures. *Holzforschung* **2000**, *54* (5), 519−527.
(43) Norgren, M.; Lindström, B. Physico-Chemical Characterization of a Fractionated Kraft Lignin. *Holzforschung* **2000**, *54* (5), 528−534.
(44) Holmberg, K.; Jönsson, B.; Kronberg, B.; Lindman, B. *Surfactants and Polymers in Aqueous Solution*; Wiley, 2002, pp 1−545..
(45) Crouvisier-Urion, K.; Bodart, P. R.; Winckler, P.; Raya, J.; Gougeon, R. D.; Cayot, P.; Domenek, S.; Debeaufort, F.; Karbowiak, T. Biobased Composite Films from Chitosan and Lignin: Antioxidant Activity Related to Structure and Moisture. *ACS Sustain. Chem. Eng.* **2016**, *4* (12), 6371−6381.
(46) Wenzel, R. N. Resistance of Solid Surfaces to Wetting by Water. *Ind. Eng. Chem.* **1936**, *28* (8), 988−994.
(47) Crouvisier-Urion, K.; Lagorce-Tachon, A.; Lauquin, C.; Winckler, P.; Tongdeesoontorn, W.; Domenek, S.; Debeaufort, F.; Karbowiak, T. Impact of the Homogenization Process on the Structure and Antioxidant Properties of Chitosan-Lignin Composite Films. *Food Chem.* **2017**, *236*, 120−126.
(48) Rukmanikrishnan, B.; Ramalingam, S.; Rajasekharan, S. K.; Lee, J.; Lee, J. Binary and Ternary Sustainable Composites of Gellan Gum, Hydroxyethyl Cellulose and Lignin for Food Packaging Applications: Biocompatibility, Antioxidant Activity, UV and Water Barrier Properties. *Int. J. Biol. Macromol.* **2020**, *153*, 55−62.
(49) Gadioli, R.; Morais, J. A.; Waldman, W. R.; De Paoli, M.-A. The Role of Lignin in Polypropylene Composites with Semi-Bleached Cellulose Fibers: Mechanical Properties and Its Activity as Antioxidant. *Polym. Degrad. Stab.* **2014**, *108*, 23−34.
(50) Lai, W.-F. Design of Polymeric Films for Antioxidant Active Food Packaging. *Int. J. Mol. Sci.* **2021**, *23* (1), 12.
(51) Domínguez-Robles, J.; Cuartas-Gómez, E.; Dynes, S.; Utomo, E.; Anjani, Q. K.; Detamornrat, U.; Donnelly, R. F.; Moreno-Castellanos, N.; Larrañeta, E. Poly(Caprolactone)/Lignin-Based 3D-Printed Dressings Loaded with a Novel Combination of Bioactive Agents for Wound-Healing Applications. *Sustainable Mater. Technol.* **2023**, *35*, No. e00581.
(52) Reesi, F.; Minaiyan, M.; Taheri, A. A Novel Lignin-Based Nanofibrous Dressing Containing Arginine for Wound-Healing Applications. *Drug Delivery Transl. Res.* **2018**, *8* (1), 111−122.
(53) Xu, J.; Xu, J. J.; Lin, Q.; Jiang, L.; Zhang, D.; Li, Z.; Ma, B.; Zhang, C.; Li, L.; Kai, D.; Yu, H.-D.; Loh, X. J. Lignin-Incorporated Nanogel Serving As an Antioxidant Biomaterial for Wound Healing. *ACS Appl. Bio Mater.* **2021**, *4* (1), 3−13.
(54) Lin, N.; Fan, D.; Chang, P. R.; Yu, J.; Cheng, X.; Huang, J. Structure and Properties of Poly(Butylene Succinate) Filled with Lignin: A Case of Lignosulfonate. *J. Appl. Polym. Sci.* **2011**, *121* (3), 1717−1724.

(55) Liu, L.-Y.; Hua, Q.; Renneckar, S. A Simple Route to Synthesize Esterified Lignin Derivatives. *Green Chem.* **2019**, *21* (13), 3682−3692.
(56) Krekeler, C.; Ziehr, H.; Klein, J. Physical Methods for Characterization of Microbial Cell Surfaces. *Experientia* **1989**, *45* (11−12), 1047−1055.
(57) Li, B.; Logan, B. E. Bacterial Adhesion to Glass and Metal-Oxide Surfaces. *Colloids Surf., B* **2004**, *36* (2), 81−90.
(58) van Loosdrecht, M. C.; Lyklema, J.; Norde, W.; Schraa, G.; Zehnder, A. J. The Role of Bacterial Cell Wall Hydrophobicity in Adhesion. *Appl. Environ. Microbiol.* **1987**, *53* (8), 1893−1897.
(59) Maikranz, E.; Spengler, C.; Thewes, N.; Thewes, A.; Nolle, F.; Jung, P.; Bischoff, M.; Santen, L.; Jacobs, K. Different Binding Mechanisms of Staphylococcus Aureus to Hydrophobic and Hydrophilic Surfaces. *Nanoscale* **2020**, *12* (37), 19267−19275.
(60) Thewes, N.; Loskill, P.; Jung, P.; Peisker, H.; Bischoff, M.; Herrmann, M.; Jacobs, K. Hydrophobic Interaction Governs Unspecific Adhesion of Staphylococci: A Single Cell Force Spectroscopy Study. *Beilstein J. Nanotechnol.* **2014**, *5*, 1501−1512.
(61) Spengler, C.; Thewes, N.; Jung, P.; Bischoff, M.; Jacobs, K. Determination of the Nano-Scaled Contact Area of Staphylococcal Cells. *Nanoscale* **2017**, *9* (28), 10084−10093.
(62) Aradmehr, A.; Javanbakht, V. A Novel Biofilm Based on Lignocellulosic Compounds and Chitosan Modified with Silver Nanoparticles with Multifunctional Properties: Synthesis and Characterization. *Colloids Surf., A* **2020**, *600*, 124952.
(63) Djajadi, D. T.; Brenelli, L. B.; Franco, T. T.; Thygesen, L. G.; Jørgensen, H. Lignosulfonate Properties and Reaction Conditions Enhance Precipitation and Affect Ensuing Quality of Proteins from Green Biomass Juice for Monogastric Animal Feed. *Anim. Feed Sci. Technol.* **2022**, *285* (115212), 115212.
(64) Semeraro, E. F.; Devos, J. M.; Porcar, L.; Forsyth, V. T.; Narayanan, T. In Vivo Analysis of the Escherichia Coli Ultrastructure by Small-Angle Scattering. *IUCrJ* **2017**, *4*, 751−757.
(65) Harris, L. G.; Foster, S. J.; Richards, R. G.; Lambert, P.; Stickler, D.; Eley, A. An Introduction to Staphylococcus Aureus, and Techniques for Identifyingand Quantifying S. Aureus Adhesins in Relation to Adhesion to Biomaterials:Review. *Eur. Cells Mater.* **2002**, *4*, 39−60.
(66) Kreve, S.; Reis, A. C. D. Bacterial Adhesion to Biomaterials: What Regulates This Attachment? A Review. *Jpn. Dent. Sci. Rev.* **2021**, *57*, 85−96.
(67) Salas, C.; Rojas, O. J.; Lucia, L. A.; Hubbe, M. A.; Genzer, J. On the Surface Interactions of Proteins with Lignin. *ACS Appl. Mater. Interfaces* **2013**, *5* (1), 199−206.
(68) Platnieks, O.; Gaidukovs, S.; Neibolts, N.; Barkane, A.; Gaidukova, G.; Thakur, V. K. Poly(Butylene Succinate) and Graphene Nanoplatelet-Based Sustainable Functional Nanocomposite Materials: Structure-Properties Relationship. *Mater. Today Chem.* **2020**, *18*, 100351.
(69) Wang, X.; Zhou, J.; Li, L. Multiple Melting Behavior of Poly(Butylene Succinate). *Eur. Polym. J.* **2007**, *43* (8), 3163−3170.

https://doi.org/10.1021/acsapm.3c02103
ACS Appl. Polym. Mater. 2024, 6, 1169−1181